Electronic Supplementary Material (ESI) for Journal of Materials Chemistry A.

Supporting Information

Nanostructured Polymeric Yolk-shell Capsules: a Versatile Tool for Hierarchical Nanocatalyst Design

Noelia M. Sanchez-Ballester [†] [a,b], Gaulthier Rydzek [†] [a,c]*, Amir Pakdel [a], Anjaneyulu Oruganti [d], Kotone Hasegawa [a], Masanori Mitome [a], Dmitri Golberg [a], Jonathan P. Hill [a], Hideki Abe [d], Katsuhiko Ariga [a]*

[a] World Premier International (WPI) Research Center for Materials Nanoarchitectonics (MANA), National Institute for Materials Science (NIMS), 1-1 Namiki, Tsukuba 305-0044, Japan

E-mails: RYDZEK.Gaulthier@nims.go.jp , ARIGA.Katsuhiko@nims.go.jp

[b] Institut Charles Sadron, Centre National de la Recherche Scientifique, Université de Strasbourg, 23 rue du Loess, 67034 Strasbourg Cedex 2, France

[c] International Center for Young Scientists (ICYS), Tsukuba, Ibaraki 3050047, Japan

[d] Catalytic Materials Group, Environmental Remediation Materials Unit, Environment and Energy Materials Division, National Institute for Materials Science (NIMS), 1-1 Namiki, Tsukuba 305-0044, Japan

†These authors contributed equally.

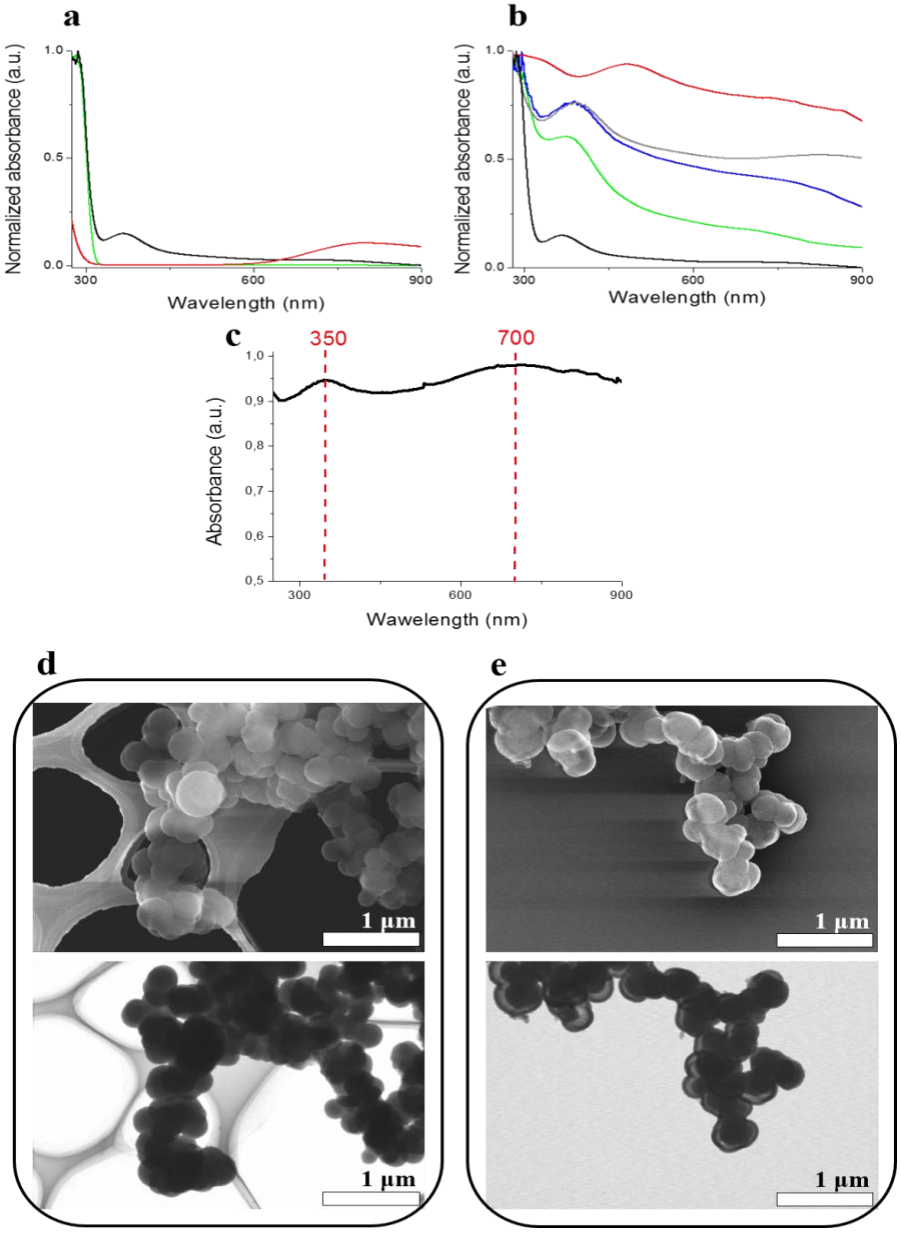

Figure S-1: Polymerization monitoring.

UV-visible absorption spectra, measured in a 95/5 w/w water/ethanol mixture, of (a) 8.7 mM $CuSO_4$ (red line), 17 mM aniline (green line) and a mixture (black line). (b) Evolution of absorption spectra of a (10 mM $CuSO_4$, 20 mM aniline, 40 mM KPS) water/ethanol mixture after 1 (black line), 15 (blue line), 60 (grey line) and 720 (red line) minutes. (c) Typical UV-Visible spectrum of the emeraldine base obtained, in a 0.5M NaOH solution. Major peaks are labelled. (d) Typical STEM micrographs in scanning and transmission modes of PANI nanostructures before (d) and after (e) purification steps.

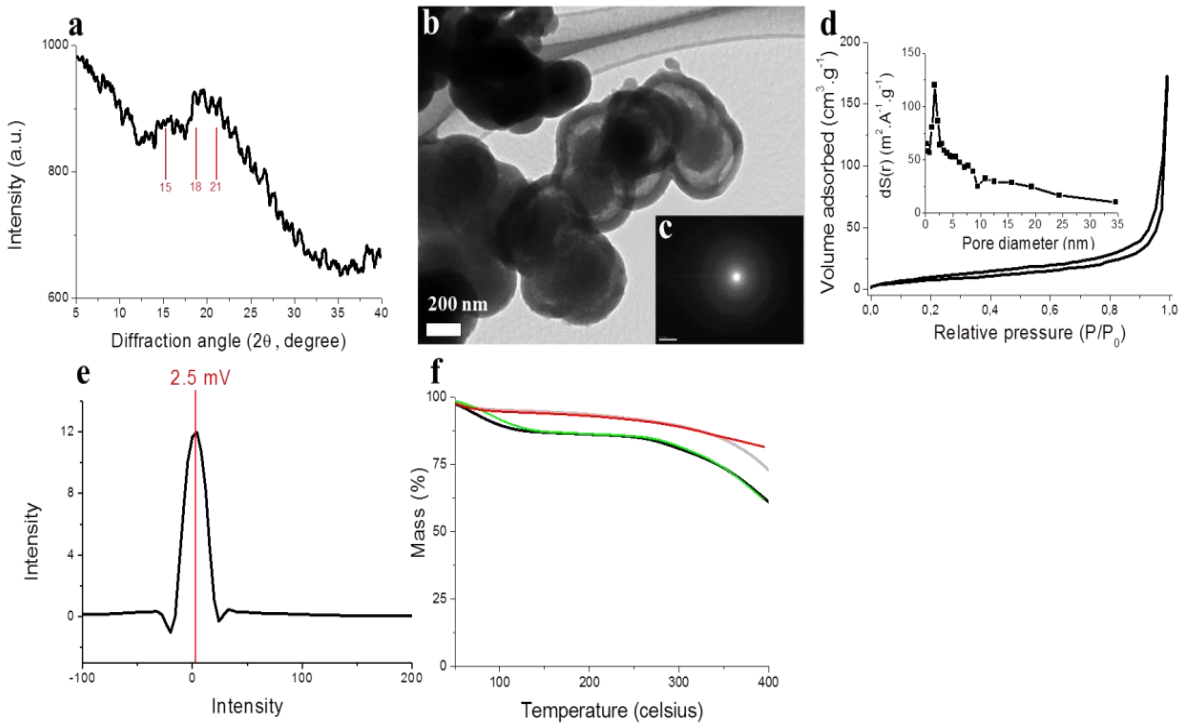

Figure S-2: general characterization of PANI yolk-shell nanocapsules.

XRD spectrum (a) and (b) typical TEM micrograph of as-prepared PANI yolk-shell nanocapsules. (c) Corresponding diffraction pattern showing absence crystallinity. (d) BET nitrogen adsorption isotherms and corresponding pore-size distribution calculated using the Barret-Joyner-Halenda method. (e) Surface zeta-potential in water of as prepared nanocapsules. (f) Thermogravimetric analysis of as prepared, and Cu-yolk Au-shell nanocapsules, before (black and green lines respectively) and after (grey and red lines respectively) formaldehyde treatment.

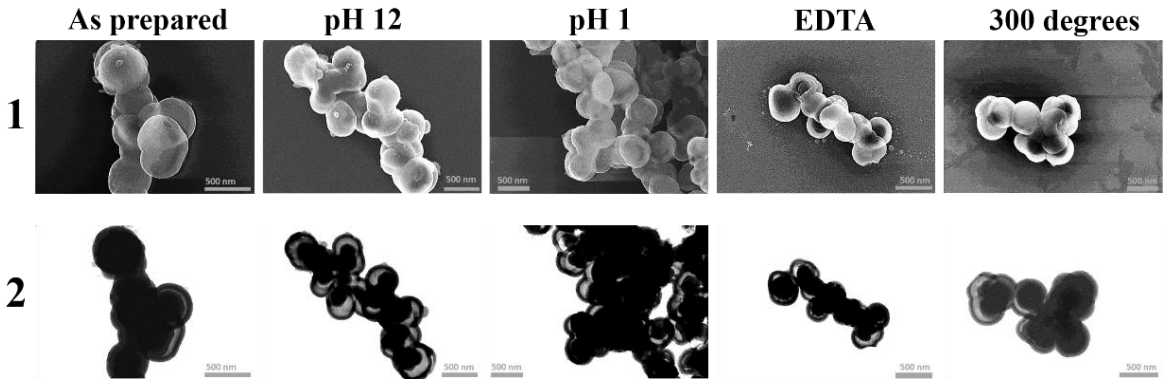

Figure S-3: robustness of nanocapsules.

Typical STEM micrographs in scanning (1) and transmission (2) modes of PANI yolk-shell nanocapsules after various treatments. The scale bar represents 500 nm.

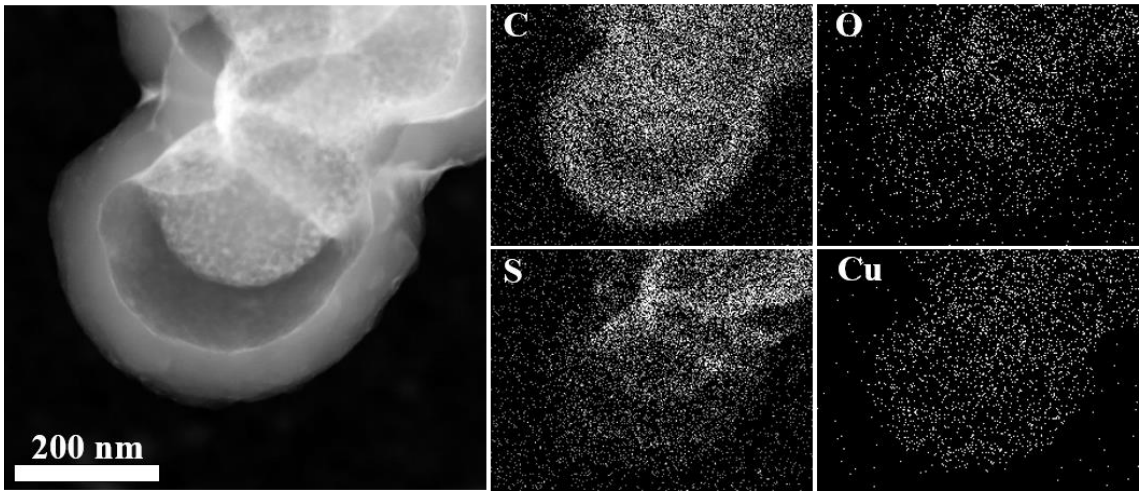

Figure S-4: composition of as prepared yolk-shell nanocapsules.

Typical TEM micrographs of as-prepared PANI yolk-shell nanocapsules and corresponding EDS analysis for carbon, oxygen, sulfur and copper elements.

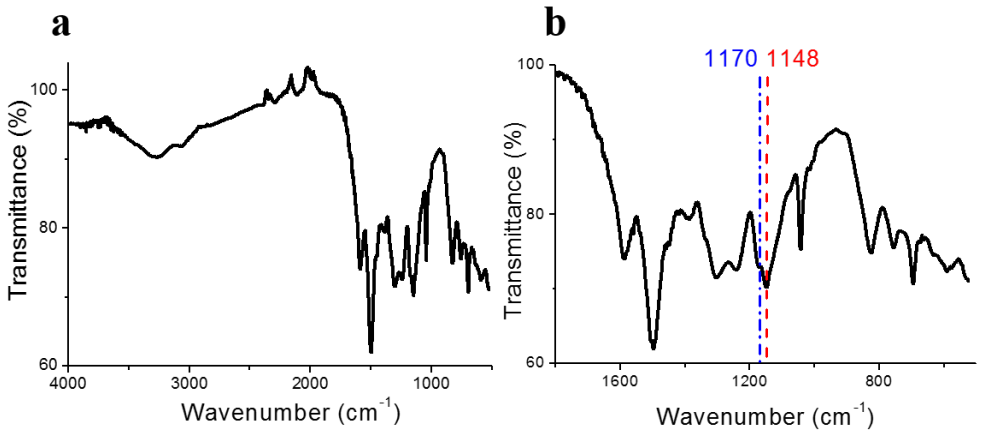

Peak (cm^{-1})	Assignment	Peak (cm^{-1})	Assignment
3300 to 3000	N-H (s)	**1290-1240**	C-N (s)
1590	C=C (s) of quinonoids	**1170** **1148**	N=Q=N band for undoped (1170) or doped (1148) PANI
1495	C=N (s) of benzenoids	**1040**	Substituted ring vibration
1390	Aromatic C=C (s)	**825**	C-H aromatic (oop)
1340	$C\text{-}N^{+}$(s), C-H (b) of quinonoids	**750**	C-H aromatic (def)

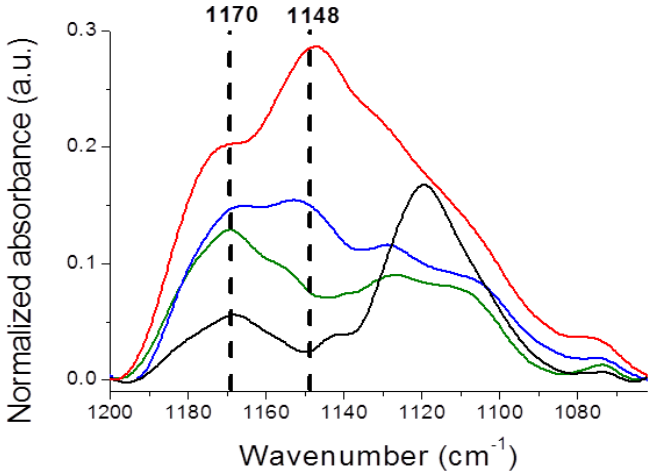

Figure S-5: ATR-FTIR spectrum of nanocapsules.

Typical ATR-FTIR spectrum (a) of as prepared nanocapsules and (b) zoom on its fingerprint region. Major peaks are labelled and assigned in the table.[1–3] Zoom on the 1170-1148 cm-1 peaks, characteristic of doped and non doped states of PANI for PANI

yolk-shell nanocapsules after loading with Cu(II) (red line), treatment with EDTA for 48h (black line), after localized copper reduction in the yolk using hydrazine (green line) and after gold shell deposition (blue line).

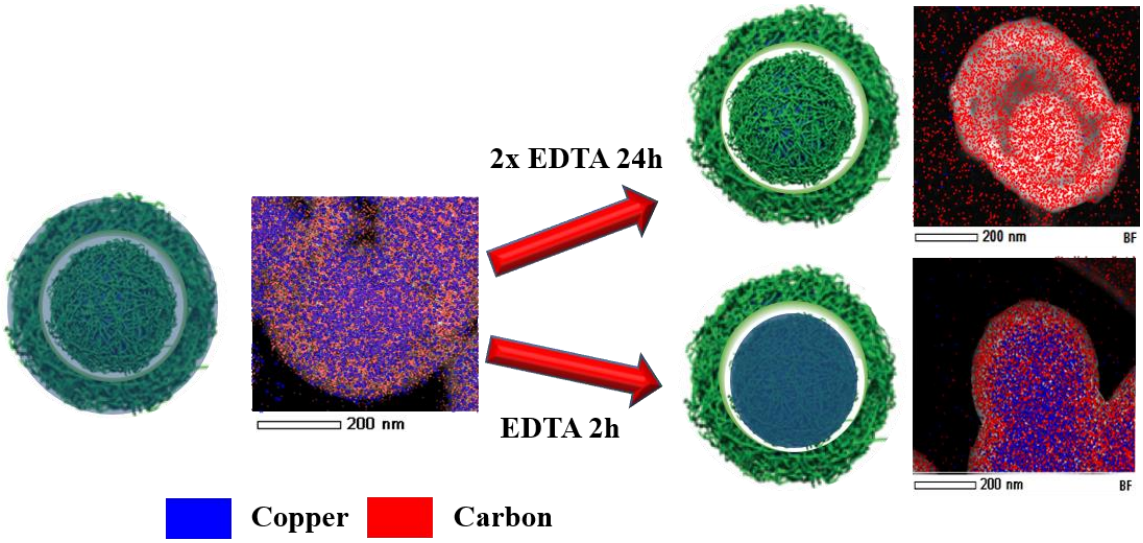

Figure S-6: Selective doping of PANI.

Schematic depiction and TEM-EDS analysis of PANI yolk-shell nanocapsules as prepared and after treatment with EDTA for 2h or 48h. The scale bar is 200 nm.

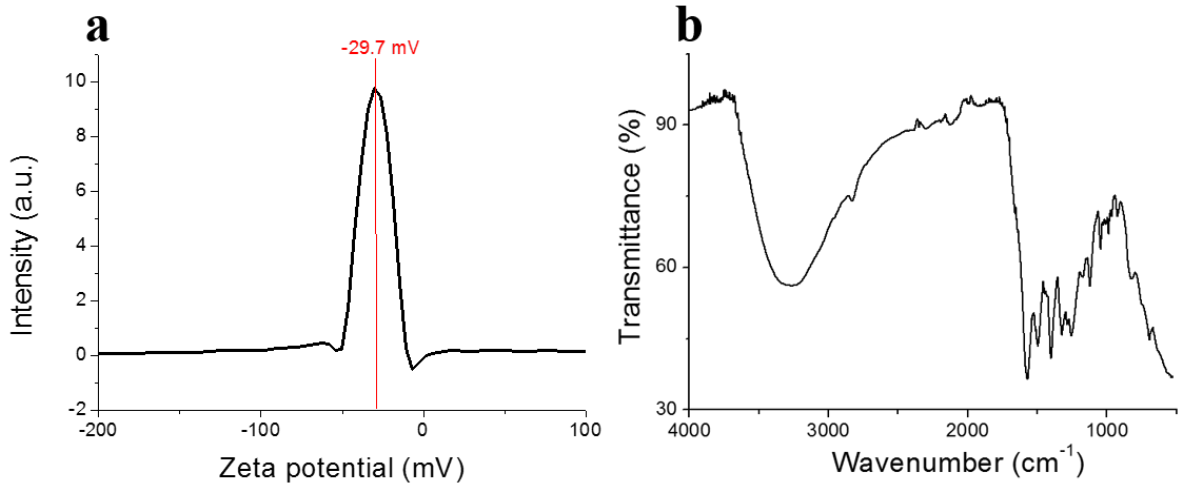

Peak (cm^{-1})	Assignment	Peak (cm^{-1})	Assignment
3600 to 2880	N-H (s) + O-H (s)	1290-1240	C-N (s)
2820	C-H (s)	**1170**	**N=Q=N band for undoped PANI**
1610-1530	C=C (s) of quinonoids COO^- (a.s. and s.)	**1120**	C-O (s)
1495	C=N (s) of benzenoids	1040	Substituted ring vibration
1400	C=O (s)	**980-960**	COO^-
1390	Aromatic C=C (s)	**920**	C-C (s)
1340	C-N^+(s), C-H (b) of quinonoids	825	C-H aromatic (oop)
1320	C-H (b)	750	C-H aromatic (def)

Figure S-7: **EDTA treatment**

(a) Intensity-zeta-potential curve of EDTA-treated PANI yolk-shell nanocapsules obtained by using flow-cell zeta-potential measurements. (b) Typical ATR-IR spectrum and corresponding peaks assignment table of PANI yolk-shell nanocapsules treated with EDTA. Peaks in bold are specifically related to EDTA trapping within PANI nanocapsules[1–3]

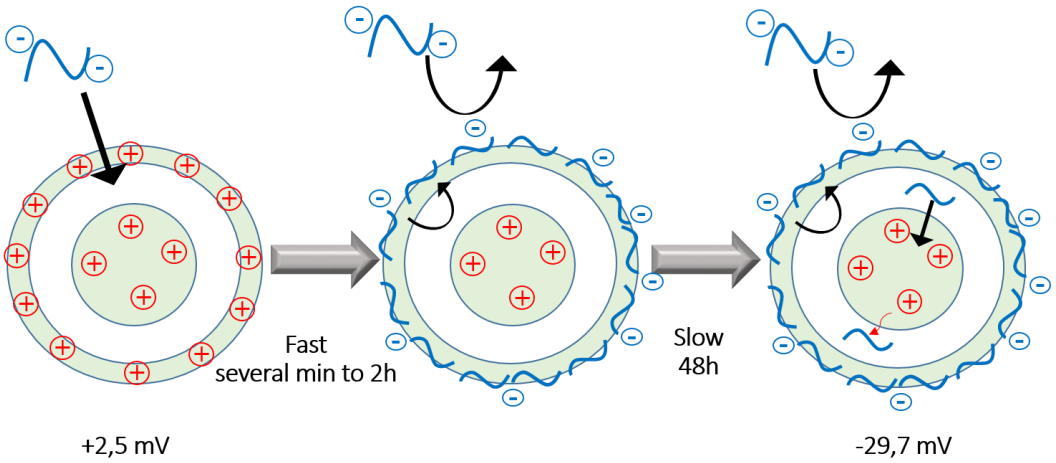

Figure S-8: **EDTA treatment and yolk-confinement.**

Schematic depiction of the kintetic yolk-confinement effect of cations in the nanocapsules. Adsorption of EDTA on the capsules induces an overcompensation of the surface charge, leading to electrostatic repulsion of new EDTA molecules by the outer shell layer.

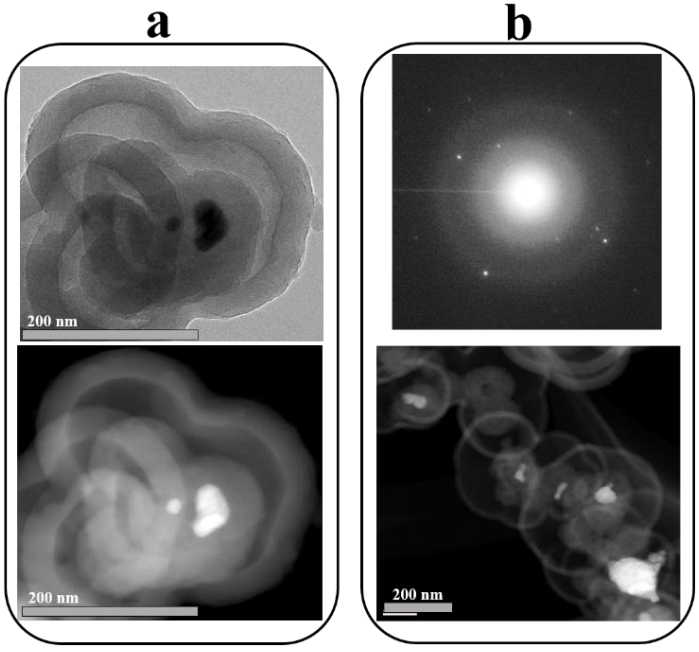

Figure S-9: reduction to Cu-yolk and (Cu-yolk Au-shell) architectures.

Typical TEM micrographs, in dark field and bright field modes, of PANI Cu-yolk nanocapsules (a,b).

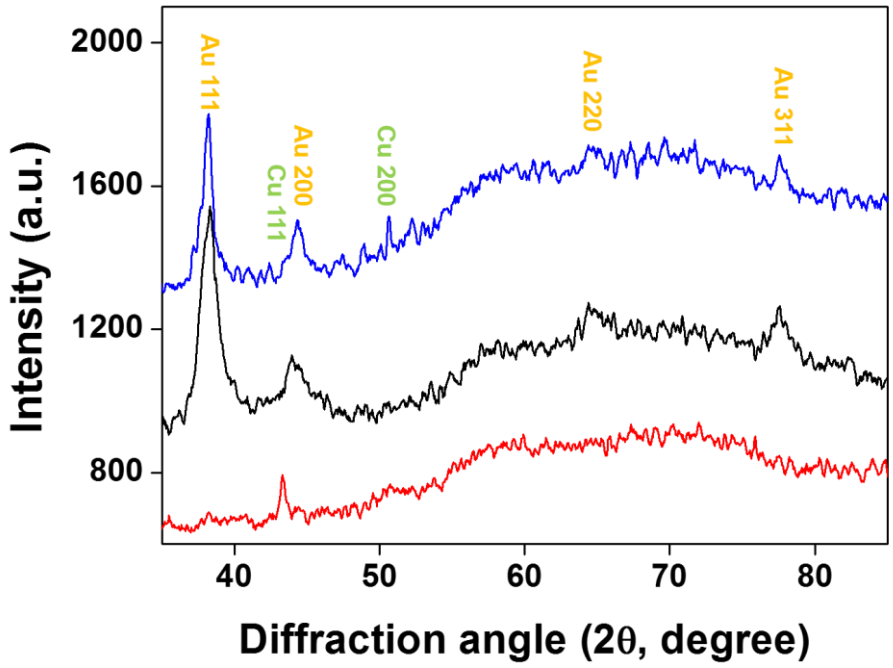

Figure S-10: reduction to cu-yolk and (cu-yolk au-shell) architectures.

Typical pXRD diffraction patterns of PANI Cu-yolk (red line), PANI Au-shell (black line) and (Cu-yolk Au-shell) nanocapsules (blue line).

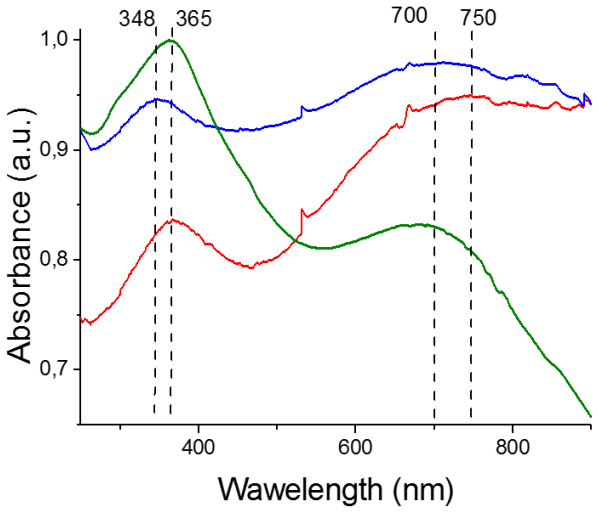

Figure S-11: reduction of nanocapsules.

Typical UV-visible spectra of PANI yolk-shell nanocapsules as prepared (blue line), after reduction by hydrazine (green line) and after abtaining the Cu-yolk Au-shell architecture (red line). Major spectral changes are labelled.

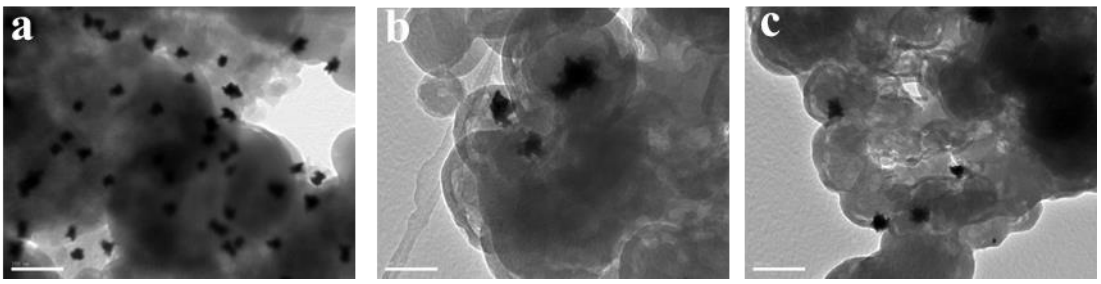

Figure S-12: gold deposition whithout formaldehyde.

Typical TEM micrographs of (Cu-yolk Au-shell) PANI nanocapsules obtained whithout using formaldehyde during the gold deposition process. Scale bares are 100 nm (a,b) and 200 nm (c).

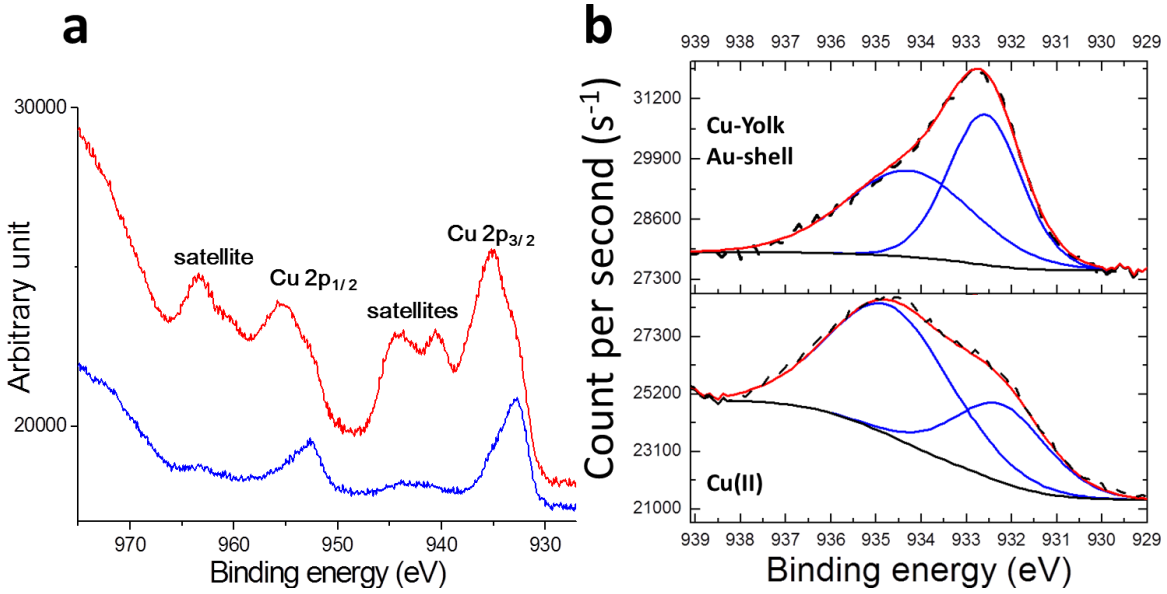

Figure S-13: XPS analysis of iron in PANI nanocapsules.

(a) Typical high resolution XPS analysis of the Cu2p area for Cu(II)-loaded PANI nanocapsules (red line) and (Cu-yolk, Au-shell) nanocapsules (blue line). (b) High resolution analysis and peak decompositon of the corresponding Cu2p3/2 area. Energies were calibrated as C1s at 285 eV.

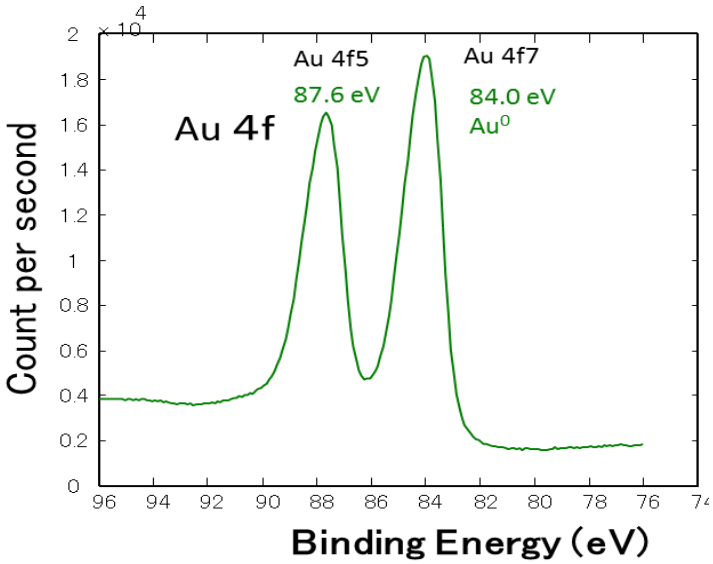

Figure S-14: XPS analysis of gold in PANI nanocapsules.

Typical high resolution XPS analysis of the Au4f area as found in (Cu-yolk, Au-shell) nanocapsules. (c) Energies were calibrated as C1s at 285 eV.

Element	As prepared	Cu core	Cu core-shell	Cu-core Au-shell	Au-shell	Ni-core	Ni core-shell	Ni-core Au-shell
Cu	3,34	3,91	10,6	2,4	0,46	0,4	0,36	0,09
Ni	0	0	0	0	0	2,1	5,22	1,5
Au	0	0	0,06	40	32,3	0	0	36

Table S-1: ICP mass abundancies (%) of Cu, Au and Ni elements in the different yolk-shell nanocapsules.

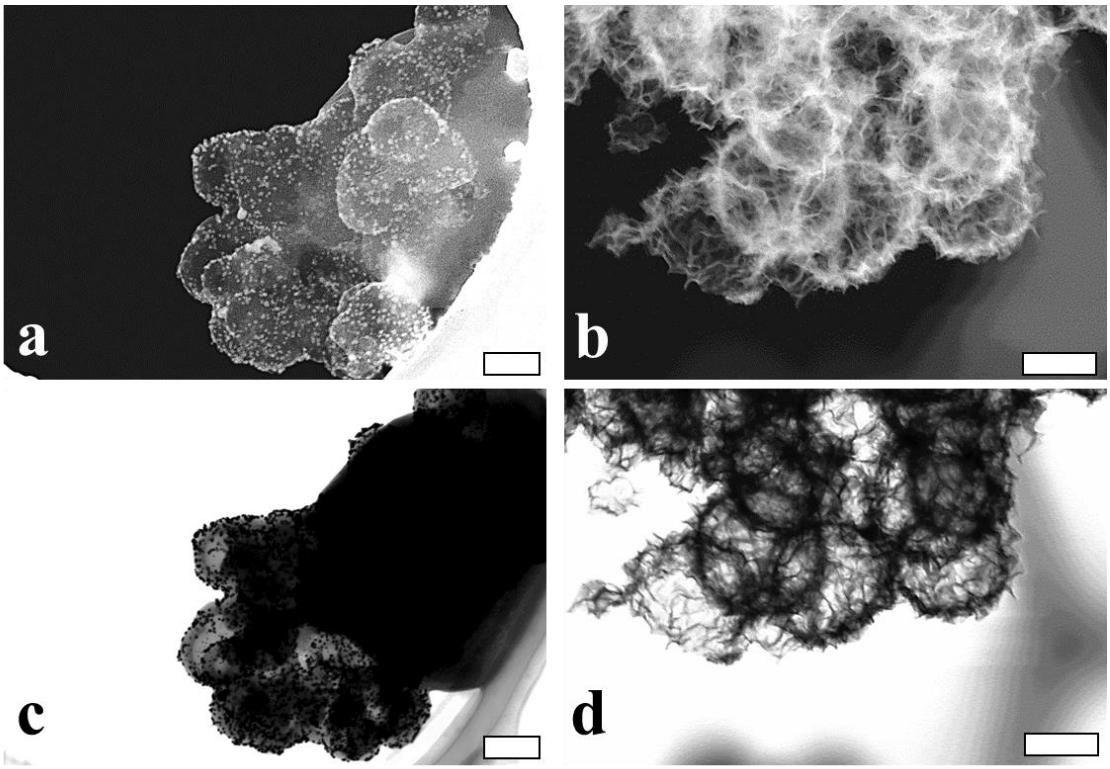

Figure S-15: Thermal stability of Cu-yolk Au-shell nanocapsules.

Typical STEM micrographs in reflection and transmission modes of (Cu-yolk Au-shell) PANI nanocapsules after thermal treatment at 300 ℃ (a,c) and 450 ℃ (b,d) The scale bar represents 200 nm.

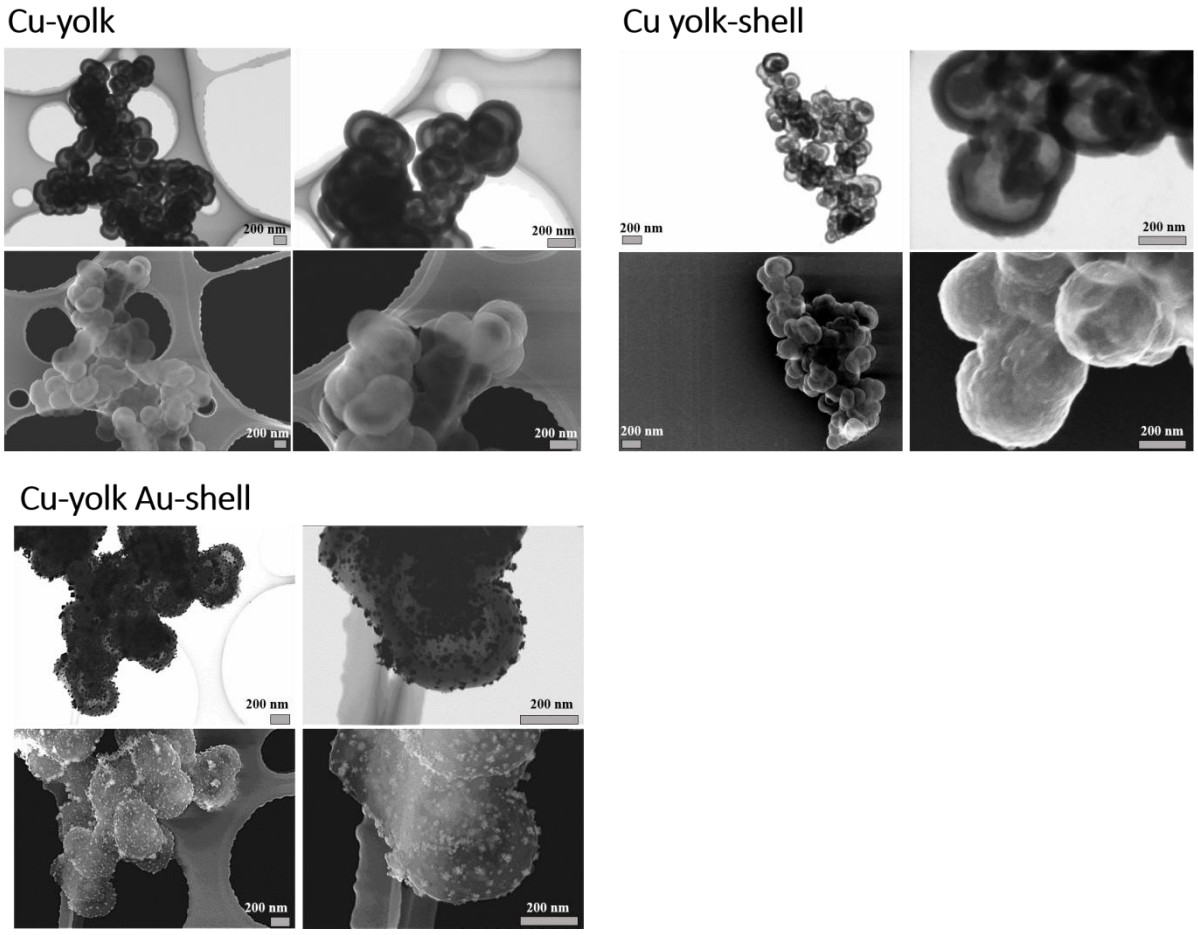

Figure S-16: formulation of copper-based architectures.

Typical STEM micrographs in reflection and transmission modes of PANI yolk-shell nanocapsules after achievement of Cu-yolk, Cu yolk-shell and (Cu-yolk Au-shell) architectures. The scale bar represents 200 nm.

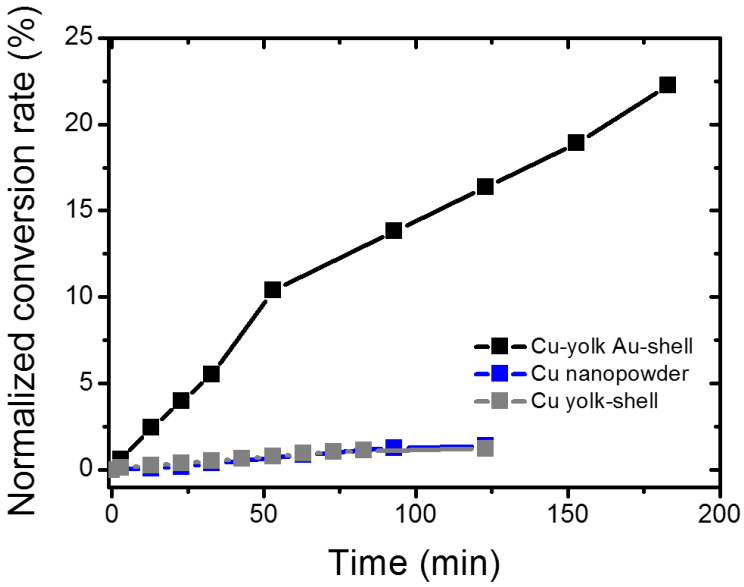

Figure S-17: Normalized oxidation rates of CO for longer times.

Oxidation rate of CO to CO_2, at 150°C, obtained with PANI yolk-shell nanocapsules functionalized as (Cu-yolk, Au-shell) (black line), non-structured Cu-yolk-shell (grey line) and copper nanopowder (blue line).

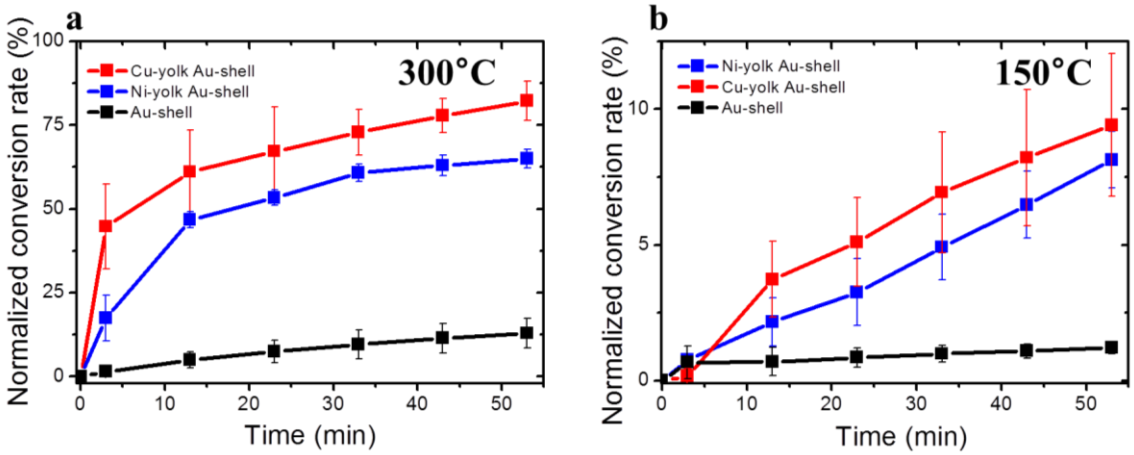

Figure S-18: CO oxidation by Au-shell capsules.

Oxidation rate of CO to CO_2 at (a) 300°*C* and (b) 150°*C,* obtained with PANI yolk-shell nanocapsules functionalized as (Ni-yolk Au-shell) (blue line), (Cu-yolk Au-shell) (red line) and Au-shell (black line). For proper comparison, datas have been normalized to a content of 1mg nickel (blue line), 1 mg copper (red line) or not normalized (black line).

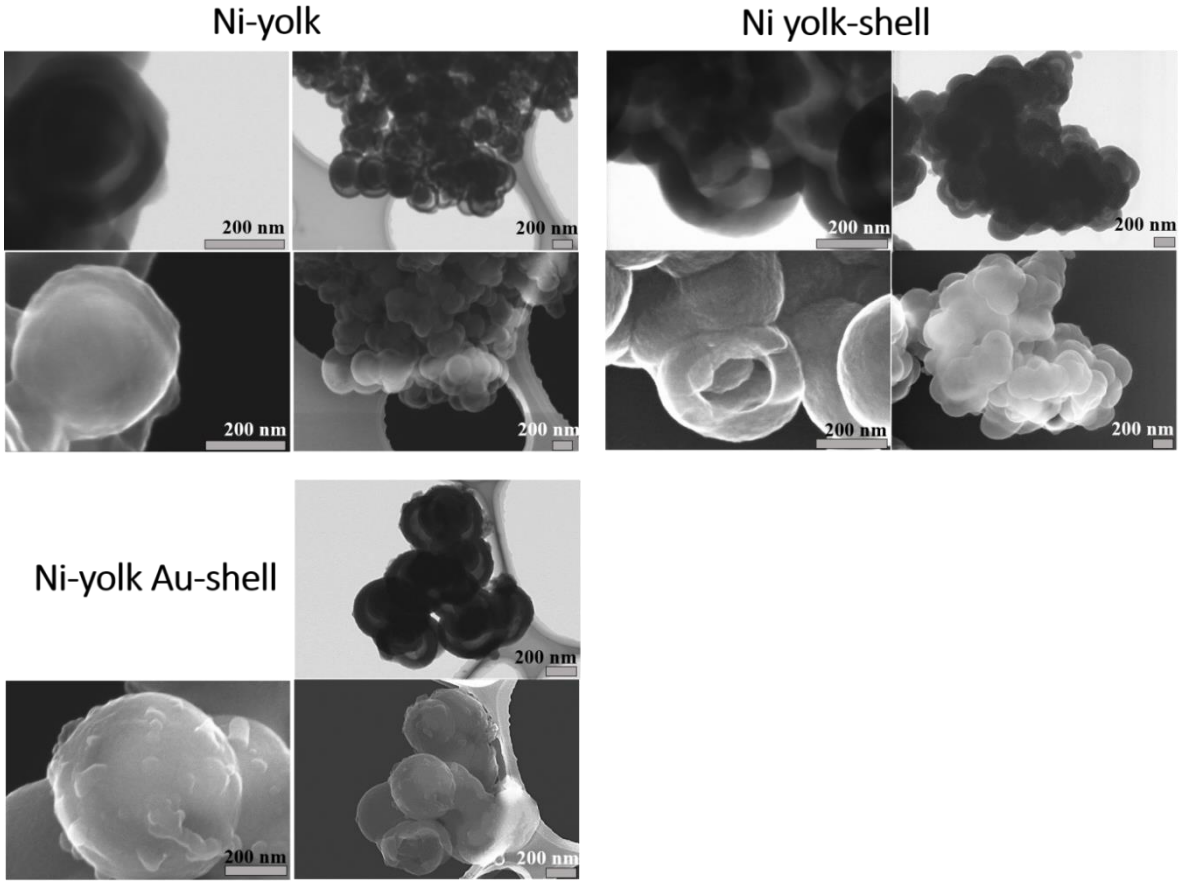

Figure S-19: formulation of nickel-based architectures.

Typical STEM micrographs in reflection and transmission modes of PANI yolk-shell nanocapsules after obtaining Ni yolk, Ni yolk-shell and (Ni-yolk Au-shell) architectures. The scale bar represents 200 nm.

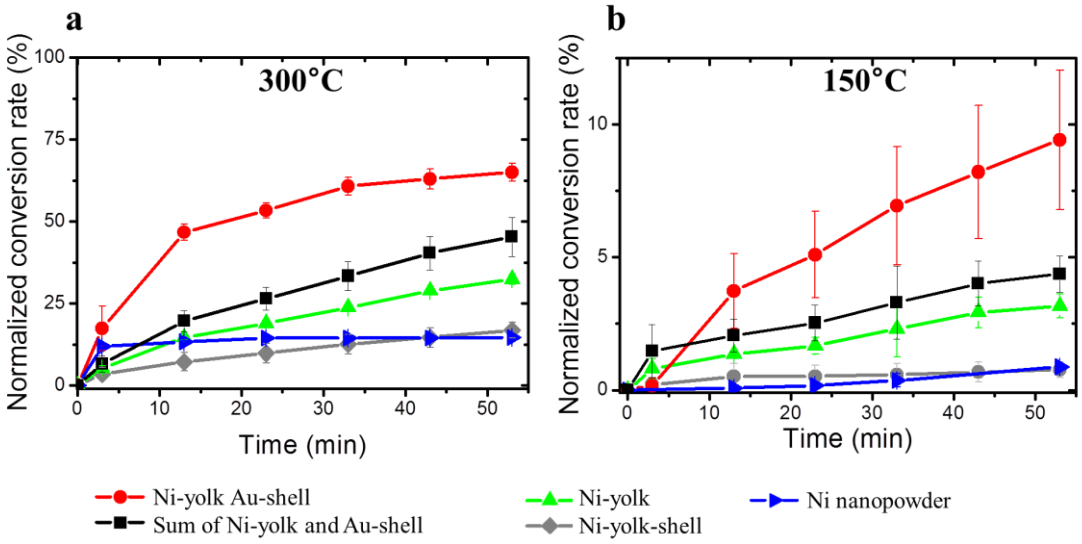

Figure S-20: CO oxidation by nickel-based yolk-shell capsules.

Oxidation rate of CO to CO_2 at (a) 300°*C* and (b) 150°*C,* obtained with a nickel nanopowder (blue line), and PANI yolk-shell nanocapsules functionalized as (Ni-yolk Au-shell) (red line), Ni-yolk (green line), Ni yolk-shell (grey line) and the sum of Ni-yolk and Au-shell performances (black line). For proper comparison, datas have been normalized to a content of 1mg nickel.

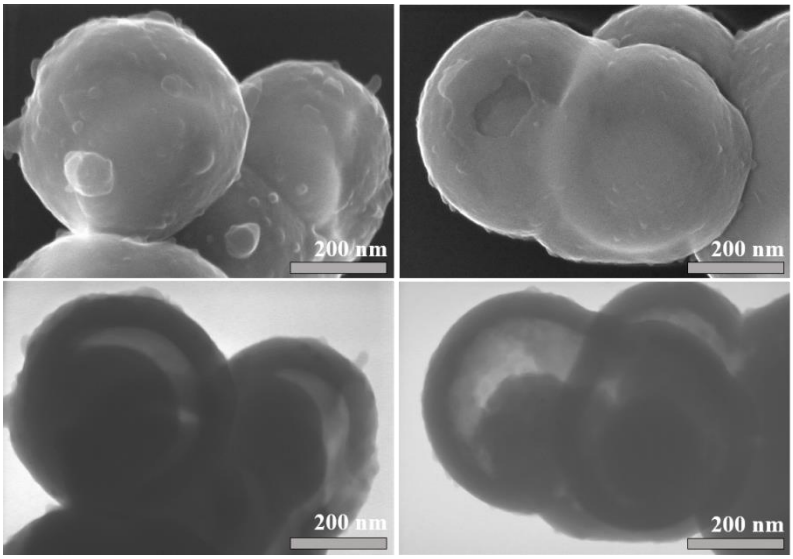

Figure S-21: generalization to platinum shell.

Typical STEM micrographs in reflection and transmission modes of PANI yolk-shell nanocapsules after deposition of Pt-shell. The scale bar represents 200 nm.

[1] Socrates, George, *Infrared and Raman Characteristic Group Frequencies Tables and Charts*, Wiley, **2001**.
[2] O. P. Dimitriev, *Polym. Bull.* **2003**, *50*, 83.
[3] C. Yang, C. Chen, *Synth. Met.* **2005**, *153*, 133.